Distance of flight of cosmic-ray muons to study dynamics of the upper muosphere

Hiroyuki K.M. Tanaka[1,2]*

1. University of Tokyo, Tokyo, Japan.
2. International Virtual Muography Institute (VMI), Global, Tokyo, Japan.

Correspondence to: Hiroyuki K.M. Tanaka

*email: ht@eri.u-tokyo.ac.jp

Abstract

The Earth can be divided by main layers, including the atmosphere, geosphere (solid Earth), and biosphere, depending on its predominant component. In this work, the layer of the Earth which constantly contains a high concentration of muons (~8×10^{12} muons) and its upper border are respectively defined as the muosphere and muopause. The altitude of the muosphere spans from the lower stratosphere to the upper crust of the Earth. In order to study its dynamics, the muopause height was spatiotemporally studied with a new kind of technique called the distance of flight (DOF) which utilizes variations in the muon's decay length. In this work, (A) numerical modeling was performed, and it was clarified that seasonal variations in the cosmic muon flux are predominantly ruled by muopause dynamics, (B) the muon data were compared with the balloon-based measurement results, and it was confirmed that muopause dynamics is closely related with lower-stratospheric height variations. Since the muopause is the region spanning between the upper troposphere and the lower stratosphere, the potential of the current distant of flight (DOF) RC2 approach needs to be further investigated by cross-comparing related case studies and other atmospheric climate datasets.

Introduction

~~The Earth can be divided into its main layers including the atmosphere, geosphere (solid Earth), biosphere, depending on its predominant component: gas in the atmosphere, solid rock/metal in the geosphere, biological activities in the biosphere.~~ RC2 Muons are

secondary particles generated in the Earth's atmosphere as a result of hadronic interactions between the incident primary cosmic rays (primaries) and atmospheric nuclei such as nitrogen and oxygen. These primaries rarely ~~usually do not~~ RC2 interact with matter within the top region of the Earth's atmosphere due to the low number density of atmospheric nuclei. However, as primaries' injection depth increases, the density of the atmosphere increases, and these primaries increasingly ~~start to~~ RC2 interact with nuclei, producing mesons such as charged pions and kaons which eventually decay into muons. Once these mesons decay into muons, there will generally be no further interaction to generate new particles since muons do not strongly interact with matter since muons undergo only electromagnetic and weak interactions but not strong nuclear interactions. RC2 Therefore, muons are extensively produced within particular altitude regions of the atmosphere. The muons' production rate increases as a function of the atmospheric depth such that: <0.01%, ~0.2%, ~2%, ~30%, and ~80% (of the entire muons we observe at sea level) up to an atmospheric depth of 5 hPa, 10 hPa, 50 hPa, 100 hPa, and 200 hPa, respectively, and almost all muons are generated up to an atmospheric depth of 300 hPa (Particle Data Group, 2022; Boezio *et al*., 1999; Boezio *et al*., 2000). On the other hand, due to ~~its~~ their RC2 strong penetration power, the muons also exist in the geosphere with a rock/water depth up to ~5/~10 km. Consequently, muons are predominant in the region defined on the altitude coordinate as ranging from 30 km and -10 km which also partly overlaps with regions of the humanosphere. This region (from +30 km to -10 km from sea level) is here defined as the muosphere. Accordingly, the muopause is defined as the upper boundary of the muosphere (as with the tropopause defining the upper boundary of the troposphere) which is located at 30 km asl. The key characteristics of the muons within the muosphere are: (A) an abundance of ~8.0×10^{12} RC1 CC1 CC2 muons* with the number RC2 of ~5×10^{3} muons km^{-3} are constantly present in the muosphere, (B) ~8×10^{16} muons are generated in the muosphere every second and (C) ~5×10^{16} muons arrive at sea level every second. The exception to this would be neutrino-induced muons which exist throughout the geosphere (Particle Data Group, 2022), but the number RC2 of these neutrino-induced particles within the geosphere is too small (< 10^{-9} muons km^{-3}) to categorize them as being part of the muosphere.

*(1.6×10^{2} $m^{-2}s^{-1}$)RC1 [averaged muon flux RC1] × (5×10^{14} m^{2}) [Earth's surface area] × (3.0×10^{4} m) RC2 [thickness of the muosphere] / (3×10^{8} ms^{-1}) [speed of muons] RC1

The thickness of the muosphere spatiotemporally fluctuates due to processes near the surface of the Earth: mainly crustal deformation and land temperature variations. Crustal

deformation alters the density of the shallow crust and local topography. When this occurs, the underground depth threshold for muons to reach will be altered; hence the position of the bottom part of the muosphere is regionally altered, but the time scale of this change is very long (over millennia). On the other hand, the near-surface temperature variations will alter the isobaric surface height near the muopause in much shorter time scales.

Since muopause height variations are closely related with the upper-tropospheric and lower-stratospheric isobaric surface height variations, studying muopause dynamics has the potential to contribute to research in this field RC2. For example, it was reported that the 2020 and 2021 ozone holes were both associated with large decreases in polar lower stratospheric heights (Yook *et al*., 2022). Sudden stratospheric warming (SSW) RC2 is characterized by large ~~geopotential height~~ isobaric surface height rises at the pole (Kretschmer *et al*., 2018). The 2022 Hunga Tonga–Hunga Ha'apai volcano eruption, Tonga resulted in a substantial injection of water vapor into the upper atmosphere (Millán *et al*., 2022; Vömel *et al*., 2022). Such changes in the atmospheric composition should have had a noticeable impact on the muopause.

The established muographic imagery techniques have been applied to natural phenomena such as volcanoes (Tanaka *et al*., 2014), cultural heritage (Morishima *et al*., 2017), tropic cyclones (Tanaka *et al*., 2022a), meteotsunami (Tanaka *et al*., 2022b), and contraband detection (Gnanvo *et al*. 2011). These techniques take advantage of known properties of muon transmission and scattering through matter. In this work, the DOF technique is added, and it will be shown that the muopause height variations can be measured with this technique based on the quantitative analysis of the time-sequential muon data. Since muons are leptons with a ~~decay constant of 2.2 microseconds, the distance traveled has an influence on the muon's survival rate. the~~ lifetime at rest is 2.2 microseconds, the actual lifetime as observed from the detector, and therefore the path traveled, is much longer by the relativistic time dilation factor, and that the latter depends on energy RC2. Consequently, the sea-level muon flux will decrease/increase as the muopause uplifts/lowers. This is the basic principle of the DOF approach. In this work, the aim was to show balloon-based lower stratospheric height variations are well reproduced by applying the DOF approach to the time-sequential muon observation data.

There are a number of reports exploring barometric and temperature effects in the muon flux (Tanaka *et al*., 2022a; Tilav *et al*. 2010; COSINE-100 Collaboration, 2020; Myssowsky and Tuwim *et al*. 1926; Blackett, 1938; The IceCube Collaboration, 2019;

Adamson *et al*., 2010; Tramontini *et al*., 2019 RC2; Blumer *et al*., 2005RC1 ~~including a recent detailed review~~ Dmitrieva *et al*. 2011 RC2). However, many of these works focus on either tropospheric barometric effect or stratospheric temperature effect. In this work, DOF approach was modeled and applied to the 1,044-day time sequential muon data to compare with the Japan Meteorological Agency's balloon data.

Tramontini, M., Rosas-Carbajal, M., Nussbaum, C., Gibert, D., Marteau, J. Middle-Atmosphere Dynamics Observed With a Portable Muon Detector. Earth and Space Science **6**, 1865-1876 (2019).

Blumer *et al*. Atmospheric Profiles at the Southern Pierre Auger Observatory and their Relevance to Air Shower Measurement. Retrieved from https://arxiv.org/abs/astro-ph/0507275 (2005).

As a result, the following ~~three~~ two RC1 major characteristics were identified: (A) seasonal variations in the muon flux due to the isobaric surface height effect are much larger than seasonal variations due to the barometric effect, therefore, (B) the isobaric surface height derived by the DOF technique is consistent with the balloon-based upper-atmosphere isobaric surface height measurement results. In this paper, a detailed description of the process to arrive these results is provided. A brief discussion of its current limitation and potential improvements are also described.

2. Muosphere and muopause

If the *abundant muon flux* is defined as ≥10 muons $m^{-2}s^{-1}sr^{-1}$, the abundant muon flux is available within the altitude region between 24.5 km above sea level (a.s.l) to 20 m below ground surface of 40 m below sea level (b.s.l). This space is hereafter defined as the "middle muosphere". The region where muons exist above the middle muosphere is called the upper muosphere, and the region where muons exist below the middle muosphere is called lower muosphere. The muon flux available in the middle muosphere and the lower muosphere on the Earth are summarized in Table 1. Vertical classification of the muosphere is shown in Figure 1 as a function of the available muon flux. The muopause is defined as the altitude region with the highest muon generation rate per unit atmospheric depth (dI/dX, where I is the muon flux, and X is the atmospheric depth). dI/dX takes maximum is ~21.5 km a.s.l. where a muon flux increases by ~40 $m^2s^{-1}sr^{-1}$ every 1 km atmospheric depth. (Figure 2). This peak is defined as the *specific muopause*. If the width of the muopause is defined the region where $dI/dX \geq 20$ $m^{-2}s^{-1}sr^{-1}km^{-1}$ (half

maximum), the muopause spans from 18 km a.s.l. to 24.5 km a.s.l. This muopause is defined as the *full-width half-maximum (FWHM) muopause*. The middle muosphere contains both atmospheric and geospheric layers.

Table 1. Available muon flux in the middle muosphere and the lower muosphere on the Earth. The data were taken from Particle Data Group (2022).

	Height (km)	Muon flux (m^{-2} sr^{-1} s^{-1})	
Upper Muosphere	30	$<10^{-2}$	
-			
Middle Muosphere	25	1.0×10^{1}	Atmosphere
	23	3.0×10^{1}	
	20	1.5×10^{2}	
	15	2.2×10^{2}	
	10	2.3×10^{2}	
	5.0	2.0×10^{2}	
	3.0	1.5×10^{2}	
	2.0	1.2×10^{2}	
	1.0	1.0×10^{2}	
	Sea level	9.0×10^{1}	-
	-0.02	1.0×10^{1}	
-			
Lower Muosphere	-0.05	2.8×10^{0}	
	-0.01	3.2×10^{-1}	
	-0.5	1.2×10^{-2}	Geosphere
	-1.0	1.2×10^{-3}	

-2.0	7.0×10^{-5}
-3.0	6.0×10^{-6}
-4.0	6.0×10^{-7}
-5.0	7.0×10^{-8}

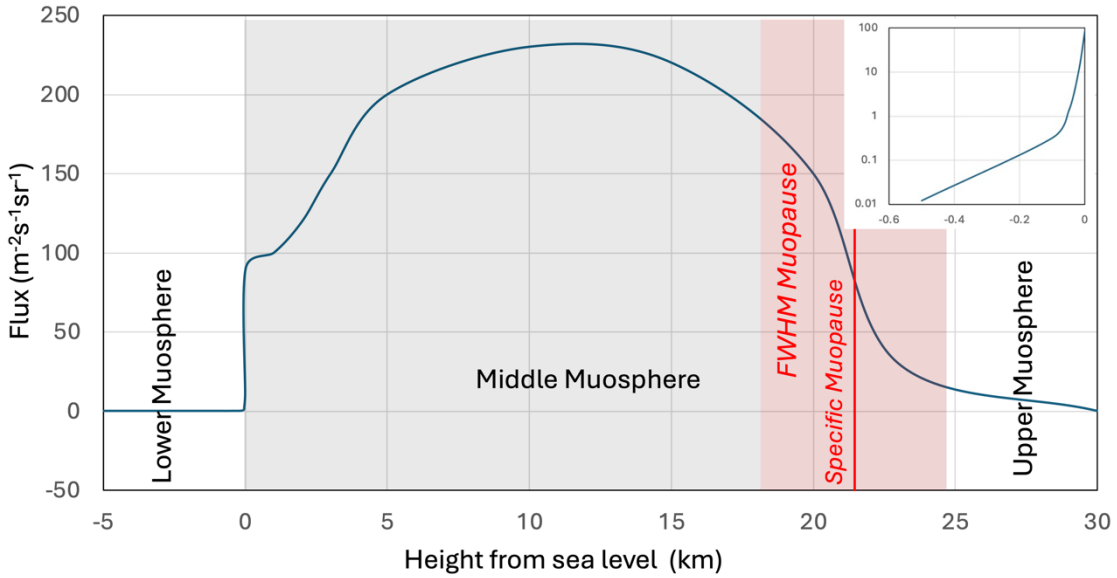

Figure 1. Configuration of the muosphere. The gray and red shaded areas respectively indicate the middle muosphere, and the FWHM muopause. The vertical red line indicates the location of the specific muosphere. The inset indicates a magnified view in the vicinity of the interface between the middle muosphere and the lower muosphere.

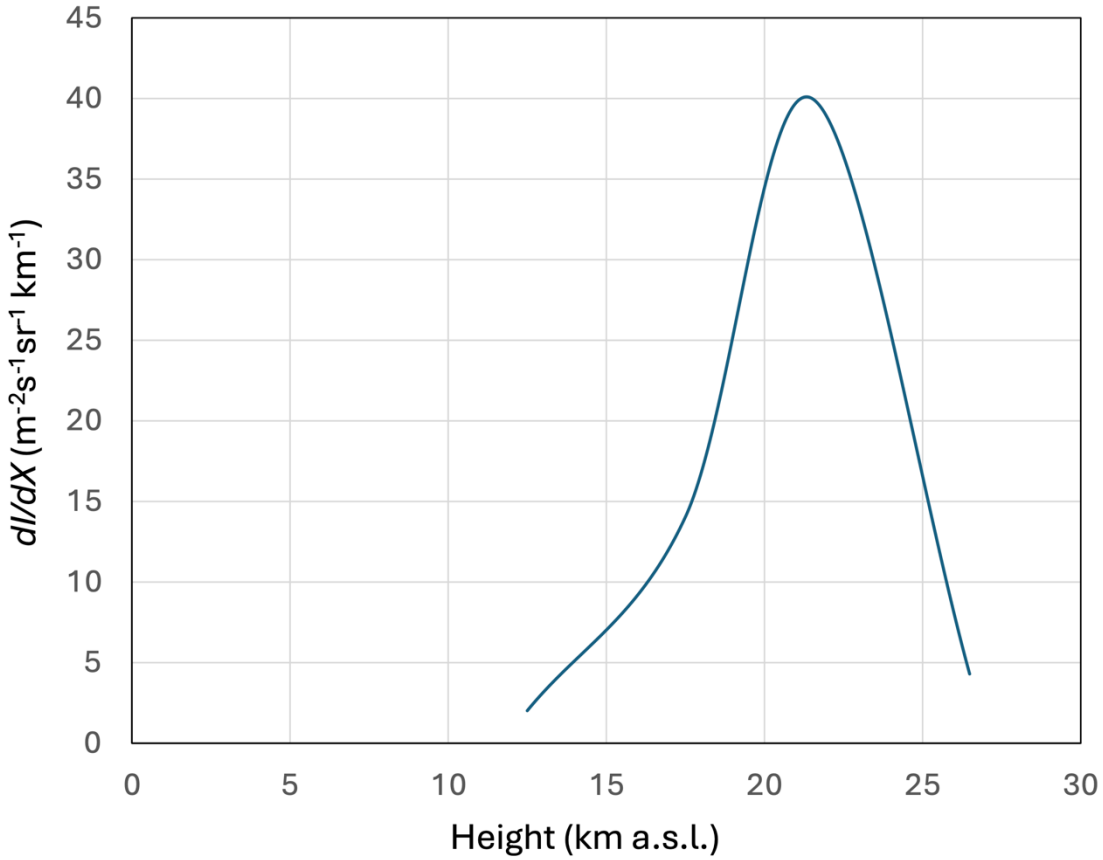

Figure 2. Muon flux gradient as a function of the altitude. RC3(1) RC1

The proposed DOF technique is similar to ground-based atmospheric LiDAR in terms of scanning the upper atmosphere. Muons are generated most extensively at the muopause that spans from the upper troposphere to the lower stratosphere. If the tropopause shifts upward, this density gradient shifts upward accordingly, and accordingly, the muopause shifts upward, then the muon's travel distance increases. The current technique measures the height of where muons are extensively generated; hence the height of the tropopause by measuring the muon's DOF. For this aspect, the DOF technique measures the dynamic (PV) tropopause height variations indirectly. (UV LiDAR measures the O_3 tropopause, and visible light LiDAR measures the cirrus cloud.) Due to the muon's strong penetrating capability, the DOF technique is not influenced by the cloud existence. RC1(1)

2. Principle of the DOF technique

The atmospheric cascades of secondary pions and kaons are developed as a result of the competition between ~~the hadronic process~~ hadronic collisions of mesons with nuclei and

the decay process of the mesons in the atmosphere RC2. Therefore, muons are not generated at a specific altitude, but instead they are generated within a certain altitude range (Boezio *et al*., 1999; Boezio *et al*., 2000).

Figure 1 shows the layer span of the muosphere on the Earth and the principle of the DOF technique. As shown in Figure 1A, the muosphere covers the region from the lower stratosphere, troposphere, and shallow region of the geosphere (shallow crust and ocean). Topography of the muopause is determined by the isobaric surface height distribution of the upper atmosphere, and is generally related to the height of tropopause. However, the tropopause region does not usually overlap with the muopause region. The isobaric surface height is high when the surface temperature is high and low in when the surface temperature is low since the larger vertical temperature gradient causes deeper convection in the troposphere, pushing the isobaric surface, upwards; hence seasonally varied. More detailed RC2 descriptions can be found later in the "Balloon-based studies near the muopause" section. As shown in Figure 1B, variations in the height of the muopause will affect the muon generation point; hence the muon's DOF. The number of muons decreases when the muopause is uplifted. If the isobaric surface height effect is comparable to or stronger than the barometric effect on the muon flux, the spatiotemporal variations in the muopause can be measured by using the local barometric data. Detailed descriptions about two essential aspects of the DOF technique, (1) modelling of the seasonal barometric effect on the muon flux and (2) modelling of the seasonal isobaric surface height effect on the muon flux, are given in the following subsections.

There are three effects that influence the muon flux: (A) variations in the muon's range due to barometric variations, (B) variations in the muopause height due to variations in mass exchange between the upper troposphere and the lower stratosphere; hence variations in the muon's distance of flight between the muopause and sea level, and (C) variations in hadronic interaction mean free paths due to stratospheric temperature variations. There are three effects in total. Effect (C) comes from the competition between the pion's and kaon's hadronic interaction mean free path (MFP) and decay length. If the stratospheric temperature increases, the air thermally expands and thus, the hadronic interaction MFP increases. However, this effect is much smaller than the other two effects since this factor is only relevant for muon flux in the energy region above 50 GeV (IceCube Collaboration, 2019) where the integrated muon intensity is lower by more than 2 orders of magnitude. Effect (A) includes variations in the muon's stopping power due to variations in their energy loss rate in the atmosphere, and variations in the muon's

decay length due to variations in their deceleration rate in the atmosphere. While there have been several works investigating the Earth's atmosphere using muons, using effect (A) (Tanaka *et al.*, 2022b; Tramontini *et al.* 2019), these previous works focused on gauging areal density variations (convertible to temperature and pressure) of the atmosphere which is conceptually close to muographic imagery. On the other hand, the DOF technique inversely using the effect (B) has never been attempted. RC2(1), RC2(2), RC2(3), RC2(5)

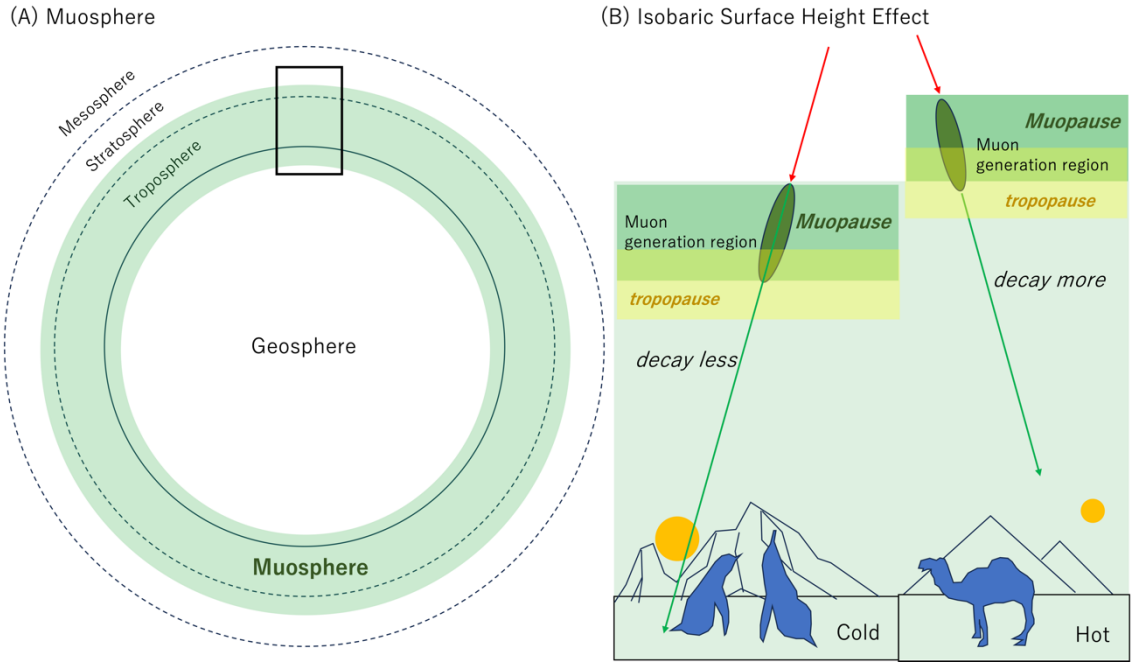

Figure 1. Definition of muosphere and the principle of the DOF technique. The span of the muosphere is shown along with other layers of the Earth (A). The black box indicates the muosphere for the region shown in (B). Red arrows and green arrows respectively indicate the primary cosmic rays and muons. Additionally, (B) shows an example of the contrast between the average height of the muopause above colder surface temperature and the height of the muopause above warner surface temperature. Dark green ovals indicate the muon production regions. As is indicated with yellow-filled boxes, the tropopause and the muopause do not exactly overlap with each other.

3. DOF Modeling

3.1 Modeling of the seasonal barometric effect on muon flux

The cosmic muon flux is also influenced by ground-level barometric variations because the amount of muon energy loss depends on the total areal density along their trajectories.

In this work, we took advantage of muon flux variations associated with the presence of a cyclone to derive variations in the muon counts in the detector as a function of the ground-level pressure in Kagoshima city. The advantage of using the cyclone data is that since the cyclone moves quickly (typically within 24 hours) and will dramatically alter the ground-level atmospheric pressure (sometimes by more than 40 hPa), barometric muon flux variations can be evaluated without being influenced from the longer-time-scale isobaric surface height effect. According to Tanaka *et al.* (2022a), the barometric correction of the muon flux can be reasonably performed by using the tropic cyclone passage events. Their reported flux drop rate is 0.0016/hPa (theory) and 0.001/hPa - 0.002/hPa (observation). This flux drop rate includes (A) the flux drop due to the higher rate of muon's absorption into the atmosphere (stop and decay), and the flux drop due to an increase in inflight decay of muons (since they lose their energy more). RC2(4), RC2(6) Figure 2A compares the temporal variations in the muon flux and the temporal variations in the ground-level atmospheric pressure induced by the 2018 Typhoon No 24. Figure 2B shows the relationship between the muon flux and the atmospheric pressure (both measured in Kagoshima city). The metrological data in Figure 2 were taken from Reference (Japan Metrological Agency, 2023). The data points in Figure 2 RC1 were fitted by a linear function and the result is shown in the following equation:

$$\Delta N = -0.0012 \Delta P \text{ [hPa]} + 2.2159. \text{ RC1} \quad (1)$$

This result indicates that the muon flux varies by 1.2% if the ground-level atmospheric pressure changes by ΔP = 10 hPa (with respect to 1,000 hPa) RC2. Since the detector used for measuring this cyclone effect on the muon flux is identical to that used for the DOF measurements, the external factors including the zenith angular dependence of the muon flux, geometrical acceptance of the detector, etc. are canceled out. The fractions of the number of the data points are respectively 60%, 82%, and 100% for deviations of $\leq 1\sigma$, $\leq 1.5\sigma$, and $\leq 2\sigma$ from the estimated line. The SD of the data points from the estimated line (6.5×10^{-4}) ~~which~~ RC2 is close to the statistical error associated with the data points (5.2×10^{-4} - 5.4×10^{-4}). The R^2 value (coefficient of determination) for this fitting was 0.85. RC2(8) The current result (0.00055/hPa -0.00185/hPa) in agreement with the flux drop rate reported in the prior work (0.001/hPa -0.002/hPa) within the error bars. RC2(6) The difference between them (0.0037) can be the fitting uncertainty which adds an uncertainty of ~18 m in estimation of the muopause height (See below). Eq. (1) was used for the barometric correction to the muon flux in the current work.

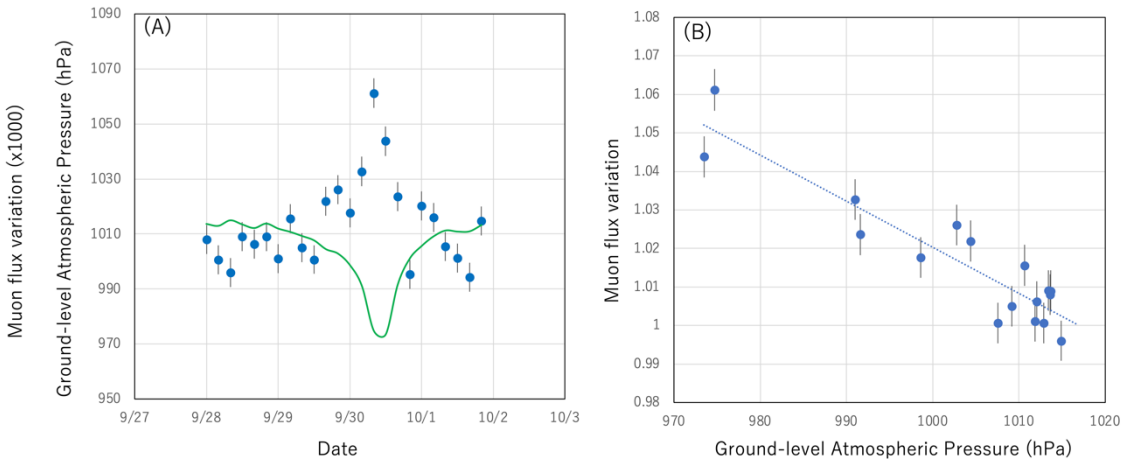

Figure 2. Variations in the muon flux induced by the ground-level atmospheric pressure variations. The muon flux variations (blue filled circles) are compared with the ground-level atmospheric pressure variations (green solid lines) induced by the 2018 Typhoon No 24 (A). The muon flux variations (blue filled circles) are shown as a function of the ground-level atmospheric pressure. The numbers on the vertical axis indicate the muon flux variation times 1,000. RC1 The dotted line indicates the linear function fitted to these data points (B).

With Eq. (1), seasonal variations of the muon flux caused by variations in the ground-level atmospheric pressure (P-driven muon flux variations) were evaluated. Figure 3A shows seasonal variations in the ground-level atmospheric pressure measured at the Kagoshima Meteorological Observatory in the period between August 2017 and August 2020. Figure 3B shows the corresponding P-driven muon flux variations based on Eq. (1).

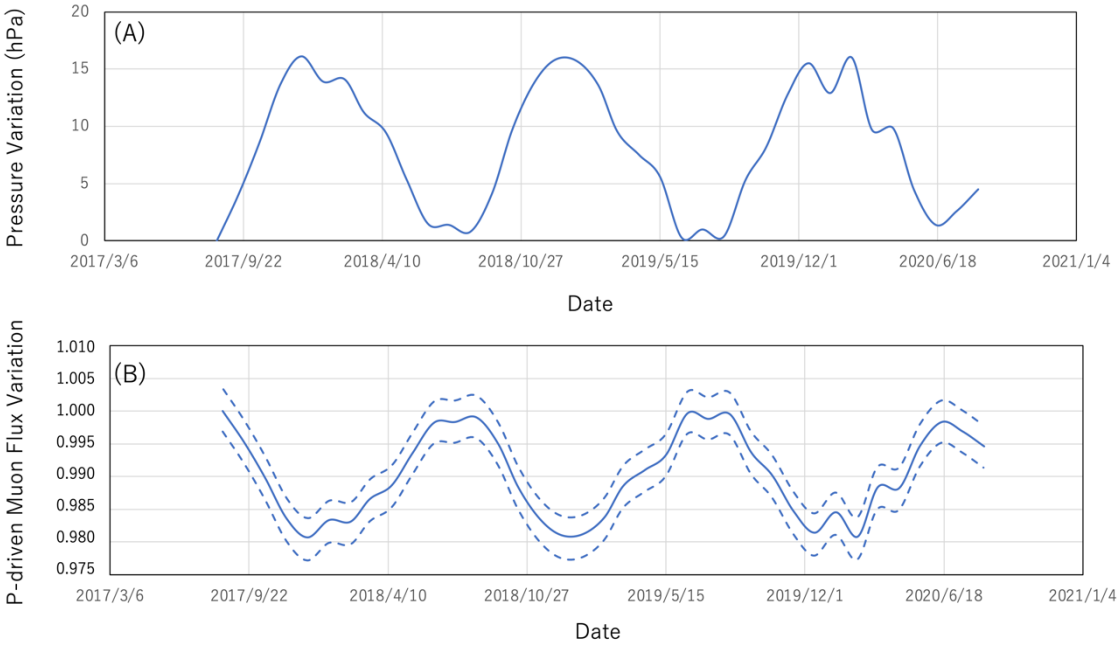

Figure 3. Seasonal variations in the ground-level atmospheric pressure (A) and estimated RC2 variations of muon flux due to variations in the ground-level atmospheric pressure (B) based on Eq. (1) RC2. The data are shown in the period between August 2017 and August 2020. The ground-level atmospheric pressure data were taken from Reference (Japan Metrological Agency, 2023). The area between dashed lines in panel (B) indicates the barometric modeling error (1 S.D.) The error values associated with the barometric data are not published by Japan Metrological Agency. RC1

3.2 Balloon-based studies of the isobaric surface height near the muopause RC2

Japan Meteorological Agency launches a balloon from Kagoshima city twice a day (09:00 and 21:00 JST) to monitor the isobaric surface height of the upper atmosphere. The monthly isobaric surface height measurement results acquired in 2018 and 2019 are shown in Figure 4 RC2. As shown in this figure, the altitude of the muopause varies ΔH ~ 500 m, reflecting seasonal variations (i.e., altitude that increases in the summer time) of the muopause. While the muon generation depth has a certain span (50-300 hPa), as can also be seen in this figure, the isobaric surface height corresponds closely with the variations in this span. Therefore, we can conclude that the isobaric structure of the upper muosphere is simply pushed further from sea level in summer and pushed closer to sea level in winter (dark green ovals in Figure 1B). Consequently, it is expected that variations in the muon survival rate at sea level is a function of the muopause height.

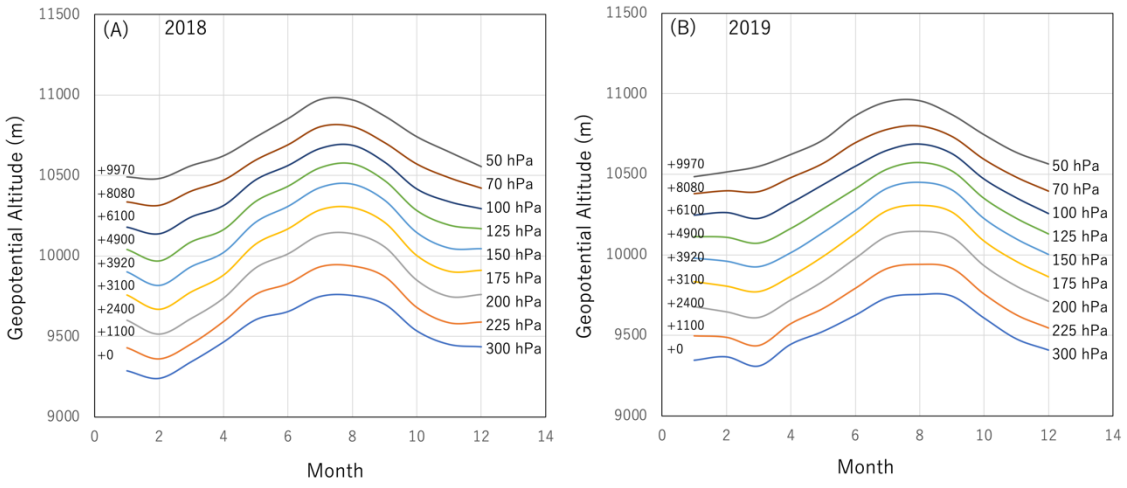

Figure 4. Seasonal changes in the ~~geopotential altitude~~ isobaric surface height RC2 of the upper troposphere and the lower stratosphere. The data acquired in 2018 (A) and the data acquired in 2019 (B) are shown. The data were taken from the Japan Metrological Agency survey (Japan Metrological Agency, 2023). The numbers on the left side of each panel indicate the offset of the altitude in units of meters.

3.3 Modeling of the seasonal isobaric surface height effect on the muon flux

As was described in the previous subsection, the isobaric surface height variations ΔH (H) are independent from H in this span. The modeling procedure is summarized as follows.

(A) The zenith-angular dependent open-sky muon spectrum data points are taken from various prior experimental works (Allkofer *et al.*, 1985; L3 Collaboration., 2004).

(B) These muon spectrum data points are interpolated to derive $I_0(E,\theta)$ by using the Thompson and Whalley analytical formula (Thompson and Whalley, 1977).

(C) Calculations of the angular-dependent muon flux are done, based on the following formula:

$$n(\theta,\phi) = \int I(E,\theta)dE, \qquad (2-1)$$

$$I(E,\theta) = I_0(E,\theta)\exp[-\Delta H(\sin\theta)^{-1}(c\tau\gamma)^{-1}](1-\Delta N), \qquad (2-2)$$

where E and θ are respectively the muon's energy, τ is the muon's decay constant RC1, and the arrival angle from zenith at sea level, $I_0(E,\theta)$ is the reference muon flux, and γ is the Lorentz factor. In Eq. (2.2), reduction of E is calculated by assuming the fixed atmospheric pressure (1013 hPa), and the effect of temporal barometric variations on dE/dX was neglected since the decay effect coming from the muon's energy loss variations due to temporal barometric variations is already incorporated into ΔN. Moreover, this decay effect in seasonal variations is small. For example, there is 15 hPa barometric variations between winter and summer (Figure 3), and these variations induce variations in energy loss of 30 MeV (in vertical), which extend/contract the muon's decay length by 190 m (in vertical) which is smaller than the muopause height variations by a factor of 3 (Figure 6). Radiative processes (i.e., bremsstrahlung, direct pair production, and photonuclear interactions) in dE/dX were neglected due to relatively long radiation length in air. RC2(4), RC2(11) Figure 5 plots Eq. (2-1) for ΔH = 0 m (Figure 5A) and ΔH = +500 m (Figure 5B). The data points are overlayed on this plot. Although it is difficult to estimate ΔH when these data were gathered, but it is assumed that ΔH = 0. It is important to note that in the current work, the quantity to be evaluated is variations in H, not H itself. RC2(9) The positive and negative signs attributed to ΔH respectively indicate respectively upward variations and downward variations. If θ approaches the value of 90°, $(\cos\theta)^{-1}$ will be diverged, so in this case, the spherical curvature of the Earth has to be considered (for θ ~90°) RC1.

(D) Calculate the number of muons recorded by the detector with:

$$N = \int_{\phi_0}^{\phi_1} \int_{\theta_0}^{\theta_1} n(\theta,\phi) d\theta d\phi, \qquad (3)$$

where θ_0, θ_1, ϕ_0, and ϕ_1 are respectively the detector's zenith (θ_0-θ_1) and azimuth (ϕ_0-ϕ_1) angular acceptance. Eq. (3) was used for the isobaric correction to the muon flux in the current work.

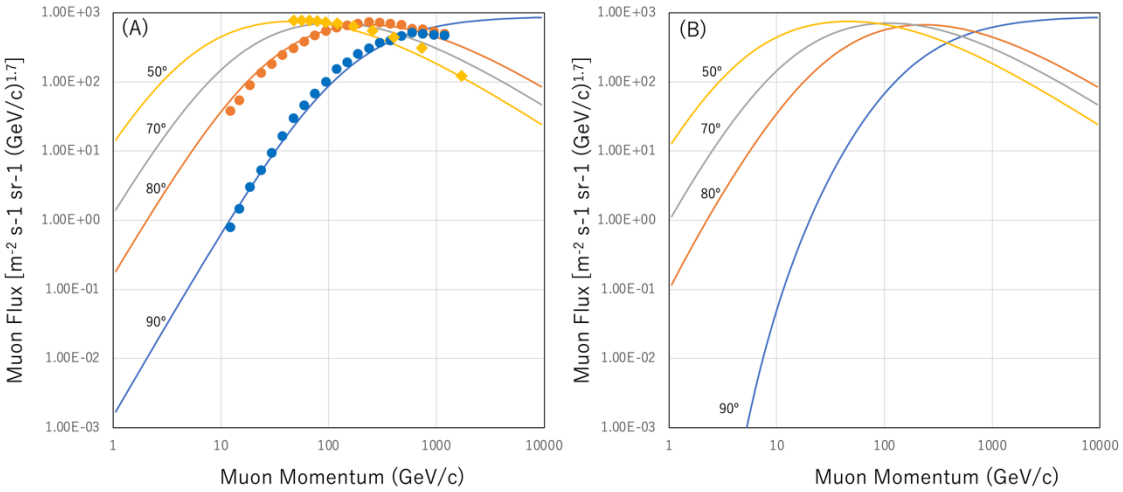

Figure 5. Differential muon flux for different isobaric surface altitudes. The spectra calculated for the reference isobaric surface altitude (ΔH = 0 m) are shown in (A) and for the case when the isobaric surface is uplifted by 500 m in (B) for various muon's arriving angles: 90° (blue), 80° (orange), 70° (gray), and 50° (yellow). Only slanted muons are shown due to the geometrical configuration of the current detector setup (see below). Filled circles and filled rhombuses are respectively the data points taken from Allkofer *et al.* (1985) and L3 Collaboration (2004). RC2(9) RC1

With Eq. (2-1), seasonal variations of the muon flux due to the isobaric surface height effect (H-driven muon flux variations) were calculated. Figure 6A shows the balloon-based ΔH value averaged over the altitudes which ranged between 50 hPa and 300 hPa. Figure 6B shows the corresponding H-driven muon flux variations based on Eq. (2-1). In order to match the angular acceptance of the tracker RC2 (described in the next section), the zenith-angular integration range of Eq. (2-1) was set to be 50°-90°. RC1 It was assumed that the muon's arriving angles are azimuthally isotropic. These results are subsequently used for the muon flux modeling process which will be described in the following subsection. As can be compared between Figure 4 and Figure 6, the seasonal isobaric surface height effect (up to 8%) is much larger (by a factor of 4) than the seasonal barometric effect (up to 2%).

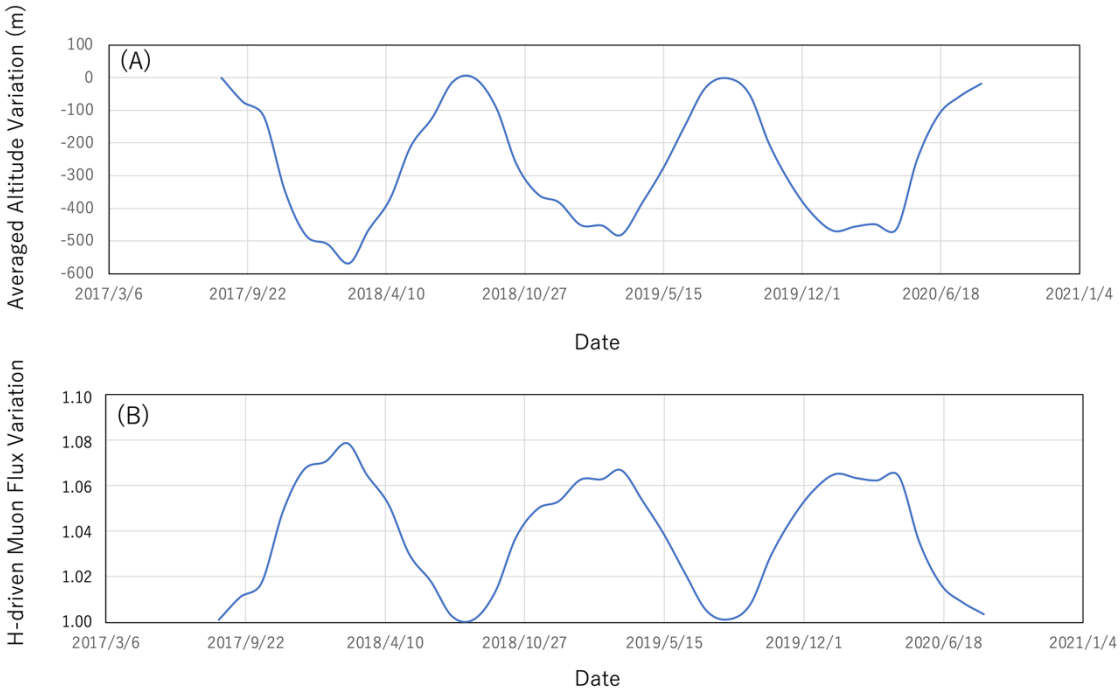

Figure 6. Balloon-based isobaric height variations averaged over the altitudes between 50 hPa and 300 hPa (A) and H-driven variations of the muon flux without the barometric correction (B). The data are shown for the period between August 2017 and August 2020. The balloon-based isobaric height data were taken from ~~Reference~~ Japan Metrological Agency (2023) RC2. The error values associated with the balloon data are not published by Japan Metrological Agency. RC1

4. Apparatus

The muon tracker used in this study consisted of 90 scintillator strip detectors. Each scintillator strip detector consisted of a plastic scintillator (Eljen EJ-200) strip connected to a photomultiplier tube (PMT; Hamamatsu R7724) via an acrylic light guide. The typical pulse height outputted from the PMTs were 3-5 V while the threshold level of the discriminator was set to be 50 mV, so that the counting rate would not be easily influenced by the drift of the PMT gain and the discriminator's threshold level caused by variations in ambient temperature. The width and the length of the plastic scintillator strip were respectively 100 mm and 1500 mm. These strips were arranged vertically and horizontally to form three position sensitive detectors (PSDs). RC1 Three PSDs were vertically arranged with a spacing of 60 cm. In order to reject electromagnetic components, such as positrons/electrons RC1 a 10-cm thick lead ~~block~~ slab concealed inside a 1.5 cm thick stainless-steel case (totaling 3 cm in thickness) ~~and a 3-cm thick stainless-steel plate~~ ~~with~~

~~a thickness of 3 cm~~ RC1 RC2 were inserted into each interval between the PSDs. A stainless-steel case is needed to protect the lead for the following reasons: (A) lead is soft, and for long-time measurements, it can be deformed, so it has to be supported by the stainless-steel case, and (B) lead is poisonous, not allowed to use it outdoor environments without coverage, so it has to be covered by the stainless-steel box. RC2(10) RC1

The best way to check the long-term detector stability is to use IBE (inverse barometric effect). Barometric variations in the muon flux are compensated by the tidal height variations since the total areal density above the detector will be constant as long as the detector is located undersea, so that the local fluctuations due to barometric variations can be intrinsically removed from the data without any artificial actions. According to the data taken at the Trance Tokyo-bay Aqua Line undersea tunnel, Japan, variations in the lunar daily muon rate was ~0.0028 (S.D.) including statical errors of ~0.001 (S.D.) for half-year measurements (Tanaka *et al.* 2021). The detector had the same configuration used in this work (R7724 and EJ200). RC2(7)

Each of the resultant PSDs consists of a segmented plane with 15 × 15 segments having a 1.5 × 1.5 m^2 active area with a spatial resolution of 10 cm. Since the distance between the uppermost stream detector and the lowermost stream detector is 120 cm, the angular resolution of this detector is 83 mrad. This angular resolution is equivalent to the spatial resolution of 830 m at a location 10 km from the tracker, but it is reduced to 8.3 km at a location 100 km from the tracker. The elevation and azimuth angular acceptance are respectively 0 ° - 51° and ±51°. However, since the active area is drastically reduced for muons injecting at higher angles with respect to PSD planes (e.g., for muons arriving at an elevation angle of 51° and an azimuth angle of 51°, the tracker's active area is reduced to 1/225), for practicality, a much smaller angular region (14 °- 32 ° for elevation angular region and ±28° for azimuthal angular region) was employed. For tracking, all vertices are examined but only the vertices that are aligned (along a straight line) are counted as an event to ensure that only muons were selected. Lead and stainless-steel shields within the detector decrease the background noise, however they also increase the possibility of muon scattering events. However, these scattering angles (10-20 mrad) are considered to be negligible in comparison to the current tracker's angular resolution (>80 mrad). The muon tracker used in the current experiment was located in Kagoshima city, Japan and it was pointed towards the southern direction. The measurement period was between August 20, 2017- June 30, 2020 (1,044 days).

5. Comparison between the model and the experimental data

Figure 7 shows the seasonal variation in the muon flux data acquired in the period between August 20, 2017- June 30, 2020. As was expected, the muon flux showed a negative correlation between the ambient temperature and the muon flux, indicating that the isobaric surface height effect is predominant in seasonal variations in the muon flux. In this period there were not any specific extraterrestrial events (such as a Forbush decrease) that could have affected the primary flux. The muon counts in each bin (bin width = 3 days) ranged between 7×10^5-7.4×10^5. The muon flux variations were normalized to the value observed on August 20, 2017. The muon flux modeling results with barometric and isobaric corrections are overlaid on this plot (red solid lines in Figure 7). The root mean square (RMS) of the deviations between the theoretical values and the observational values is ~~0.00987~~ 0.987% RC2. The measured seasonal variation in the muon flux is well explained by combining the current barometric and isobaric correction models.

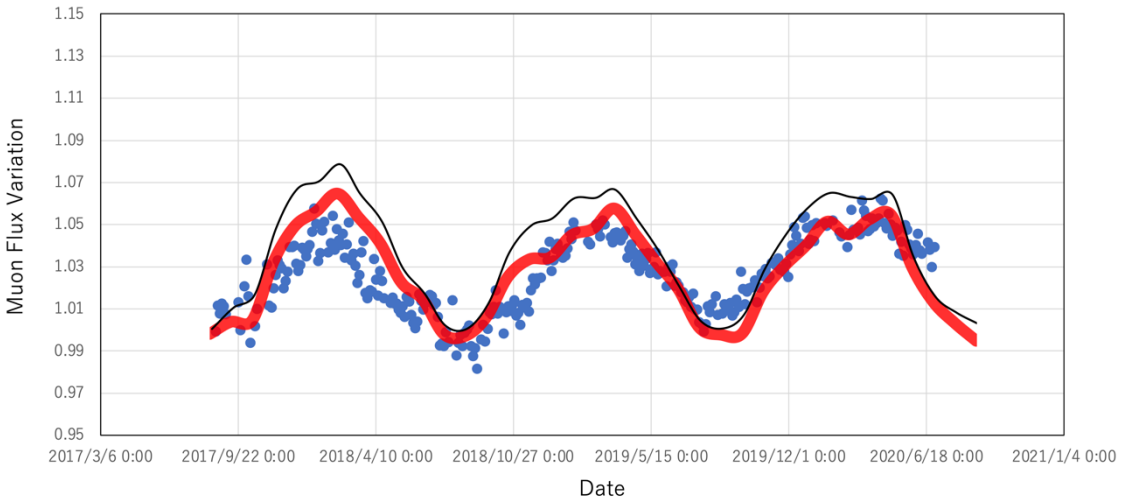

Figure 7. Seasonal variation in the muon flux data acquired in the period between August 20, 2017- June 30, 2020. The observation values (blue filled circles) and theoretical values (red solid lines) are shown. The statistical errors associated with each data point fit within the size of the circles. The barometric modelling errors are within the width of the red solid lines. Black solid lines indicate the predicted flux without the barometric correction. RC2(12)

6. Limitations and potential improvements

The RMS deviation of the observed muon flux variations from the DOF modeling results (~1%) induces an error of ~60 m in the estimation of the muopause height with the DOF technique. The DOF time resolution is 3 days. These characteristics, the accuracy and time resolution, are both significantly lower than the accuracy and the time resolution that can be attained with the GPS-loaded balloons (~5 m and 1 second). This is the main limitations of the DOF approach in its current stage of development. These limitations mainly come from (A) the statistics and (B) the modeling accuracy. Regarding factor (A), the detector size needs to be enlarged to record more muon events. In order to confirm this detector size effect, ~~further DoF measurements with larger sized detector (4.5 m^2) are currently ongoing.~~ as the first step, the detector size will be increased to a double size (4.5 m^2) to verify whether precision really scales by $2^{0.5}$, which would be a proof that statistics limitation dominates over modeling uncertainty. RC2(13) Regarding factor (B), more precise modeling developments ~~are ongoing with the extended air shower (EAS) Monte Carlo (MC) simulation.~~ with Monte Carlo (MC) simulations such as CORSIKA and Geant4 may improve the accuracy. RC2(14). The current work is based on the assumption is that the muons travel straight forwardly without experiencing scatterings; however, it must be noted that after the muons are generated near the tropopause, they travel through a material with a thickness equivalent to 20-meter water equivalent (m.w.e.) - 40 m.w.e. for the muons arriving from an elevation angular region between 14 °- 32 °, having a tendency to scatter to cause longer track lengths in the troposphere. This effect must be taken into account in our future work to make improvements to factor (B). The discrepancy between the balloon position and the muon generation region may also influence how closely the compared data sets match. The muospheric layer thickness seasonally oscillates, but its amplitude is likely to depend on location of the measurement on the Earth since the near surface temperature is regionally varied. If the surface temperature is different between the location underneath the ballon and the location underneath the region of interest of the muopause, the muopause height in this region and the balloon-based isobaric surface altitude will not coincide. Since the balloon's trajectory is random, and it is difficult to control it, the next step in development is to compare the DOF data with the satellite-based stratospheric sensing data.

7. Conclusion

In conclusion, a new muographic technique called DOF was proposed, and with this technique, it was found that the muopause height interlocks with the isobaric surface height in the upper troposphere and lower stratosphere. This work defined (A) the position

of the muopause and the layer span of the muosphere on the Earth; additionally, it was shown that (B) the muopause is located in the lower stratosphere, (C) seasonal variations in the muon flux are predominantly ruled by muopause dynamics, (D) muopause dynamics can be visualized with DOF RC2 muography by taking advantage of directional patterns of cosmic-ray muon's survival probabilities, and (E) muopause dynamics is closely related with isobaric surface height variations in the lower stratosphere.

Muopause dynamics has the potential to contribute to research focused on the upper tropospheric and lower stratospheric dynamics. In future studies, the potential of DOF RC2 muography for application to studying the dynamical processes occurring in the upper troposphere and lower stratosphere will be further investigated by performing related case studies and making specific comparisons with other atmospheric climate datasets. The next step would be spatiotemporal mapping of the muopause that would reflect spatiotemporal variations in tropospheric convection depth. RC2

REFERENCES

Adamson, P. et al. (MINOS Coll.: Observation of muon intensity variations by season with the MINOS far detector, Phys. Rev., D81, 012001, doi:10.1103/PhysRevD.81.012001, 2010

Allkofer, O.C. *et al*. Cosmic ray muon spectra at sea-level up to 10 TeV. *Nucl*. *Phys*. *B* **259**, 1-18 (1985).

Blackett, P. M. S. On the instability of the Barytron and the temperature effect of cosmic rays. *Phys*. *Rev*. **54**, 973–974 (1938). https://doi.org/10.1103/PhysRev.54.973

Boezio M. *et al*. New Measurement of the Flux of Atmospheric Muons. *Phys*. *Rev*. *Lett*. **82**, 4757 (1999).

Boezio M. *et al*. Measurement of the flux of atmospheric muons with the CAPRICE94 apparatus. *Phys*. *Rev*. *D* **62**, 032007 (2000).

COSINE-100 Collaboration. Measurement of the cosmic muon annual and diurnal flux variation with the COSINE-100 detector (2020). Retrieved from https://arxiv.org/abs/2005.13672

Dmitrieva, A.N. *et al*. Corrections for temperature effect for ground-based muon hodoscopes. *Astropart*. *Phys*. **34**, 401-411 (2011).

Gnanvo, K. *et al*. Imaging of high-Z material for nuclear contraband detection with a minimal prototype of a muon tomography station based on GEM detectors. *Nucl*. *Instr. Meth*. *A* **652**, 16-20 (2011).

Haino, S. *et al*. Measurements of primary and atmospheric cosmic-ray spectra with the BESS-TeV spectrometer. *Phys*. *Lett*. *B* **594**, 35-46 (2004).

Japan Metrological Agency. Past Metrological Data (2023). Retrieved from https://www.jma.go.jp/jma/indexe.html.

Kretschmer, M. *et al*. The different stratospheric influences on cold extremes in Eurasia and North America. *npj Clim*. *Atmos*. **1**, 44 (2018).

L3 Collaboration. Measurement of the atmospheric muon spectrum from 20 to 3000 GeV. *Phys*. *Lett*. *B* **598**, 15-32 (2004)

Millán, L. *et al*. The Hunga Tonga - Hunga Ha'apai Hydration of the Stratosphere, *Geophys*. *Res*. *Lett*. **49**, e2022GL099381 (2022).

Morishima, K., Kuno, M., Nishio, A. *et al*. Discovery of a big void in Khufu's Pyramid by observation of cosmic-ray muons. *Nature* **552**, 386–390 (2017). https://doi.org/10.1038/nature24647

Myssowsky, L., & Tuwim, L. Unregelmäßige intensitätsschwankungen der höhenstrahlung in geringer seehöhe. *Z*. *Phys*. **39**, 146–150 (1926). https://doi.org/10.1007/BF01321981

Particle Data Group, The Review of Particle Physics. *Prog*. *Theor. Exp*. *Phys*. **2022**, 083C01 (2022).

Tanaka, H. K. M., Kusagaya, T. & Shinohara, H. Radiographic visualization of magma

dynamics in an erupting volcano. *Nat. Commun.* **5**, 3381 (2014). https://doi.org/10.1038/ncomms4381

Tanaka, H.K.M., Aichi, M., Bozza, C. et al. First results of undersea muography with the Tokyo-Bay Seafloor Hyper-Kilometric Submarine Deep Detector. Sci Rep 11, 19485 (2021). https://doi.org/10.1038/s41598-021-98559-8

Tanaka, H. K. M., Gluyas, J., Holma, M. *et al*. Atmospheric muography for imaging and monitoring tropic cyclones. *Sci. Rep.* **12**, 16710 (2022a). https://doi.org/10.1038/s41598-022-20039-4

Tanaka, H. K. M., Aichi, M., Balogh, S.J. *et al*. Periodic sea-level oscillation in Tokyo Bay detected with the Tokyo-Bay seafloor hyper-kilometric submarine deep detector (TS-HKMSDD). *Sci. Rep.* **12**, 6097 (2022b). https://doi.org/10.1038/s41598-022-10078-2

The IceCube Collaboration. Seasonal variation of atmospheric muons in IceCube. *PoS* (ICRC2019) 1177 (2019). Retrieved from https://pos.sissa.it/358/894/. RC2

Thompson, M. G. & Whalley, M. R. The sea-level muon spectrum and charge ratio and their relationship with high-energy accelerator data. *J. Phys. G* **3**, 97 (1977).

Tilav, S. et al. Atmospheric variation as observed by IceCube (2010). Retrieved from arXiv:1001.0776. -> This seems not have published elsewhere.

Vömel, H. *et al*. Water vapor injection into the stratosphere by Hunga Tonga-Hunga Ha'apai, *Science* **377**, 1444–1447 (2022).

Yook, S. *et al*. Climate Impacts and Potential Drivers of the Unprecedented Antarctic Ozone Holes of 2020 and 2021. *Geophys. Res. Lett.* **49**, e2022GL098064 (2022). https://doi.org/10.1029/2022GL098064

Data Availability

The datasets used and/or analyzed during the current study are available from the corresponding author on reasonable request.

Author Contribution

H.K.M.T. wrote the text. H.K.M.T. prepared the figures. H.K.M.T. reviewed the manuscript.

Competing interests

The author is a member of the editorial board of Geoscientific Instrumentation, Methods and Data Systems.